Ferroelectric $Sr_{0.60}Ba_{0.40}Nb_2O_6$ thin films by the sol-gel process: Electrical and optical properties

Yuhuan Xu, Ching Jih Chen, Ren Xu, and John D. Mackenzie
Materials Science and Engineering Department, University of California, Los Angeles, California 90024
(Received 22 October 1990; revised manuscript received 25 January 1991)

Transparent ferroelectric strontium barium niobate (SBN) thin films were made on fused silica, silicon, and GaAs substrates by the sol-gel process. The microstructure of these thin films was studied. Preferentially oriented SBN thin films on fused silica substrates can be obtained by applying a dc electric field during heat treatment. A heterojunction effect was further confirmed by the demonstration of photocurrent. The optical, pyroelectric, ferroelectric, and electro-optic properties of the SBN films were measured. An optical refractive index of 2.31 and effective linear electric-optic coefficient of 30×10^{-12} m/V were obtained on the film.

I. INTRODUCTION

In the past 2 years, a tremendous increase of interest in ferroelectric thin films has been aroused in the ferroelectric community because of a number of recent advances in thin-film processing. Various application capabilities of ferroelectric thin films, such as in piezoelectric or electroacoustic transducers,[1,2] high-frequency surface-acoustic-wave (SAW) devices,[3] pyroelectric infrared detectors,[4–6] ferroelectric memory cells,[7,8] ferroelectric-photoconductive displays,[9–12] two-dimensional spatial light modulators or optical waveguide devices integrated onto GaAs or Si with a SiO_2 buffer-layer modulator,[13,14] ferroelectric gate [field-effect transistors (FET's)] and "MIST" (metal-insulator-semiconductor-transistors) devices,[15,16] highly complex nonvolatile and radiation hard memory circuits,[17,18] etc., have been proposed, studied, and demonstrated.

Among the ferroelectric thin films studied, SBN (strontium barium niobate solid-solution series $Sr_{1-x}Ba_xNb_2O_6$, where $0.2<x<0.8$) films are of special interest and have many important applications. They have a tetragonal tungsten-bronze- (TB-) type structure and belong to the point group with $4mm$ symmetry at room temperature. Because of the continuously variable ratio of Sr to Ba, the Curie temperature T_C of SBN can be altered in the range of 60–250 °C. At room temperature a spontaneous polarization occurs along the **c** axis of the tetragonal lattice in SBN crystal.[19]

SBN crystal possesses excellent pyroelectric and linear electro-optic effects with low half-wave voltage.[20–22] A strong photorefractive effect and two- (or four-) wave mixing in doped SBN crystals were observed.[23–25] A polycrystalline ferroelectric thin film of SBN ([Sr]/[Ba]=50/50, grain size approximately 2–3 μm) was obtained by rf sputtering. This film displays approximately the same nonlinear properties as those observed in SBN single crystals.[26]

Recently, we reported our observations of the self-biased heterojunction effect of ferroelectric thin films on silicon substrates.[27] Transparent, crack-free, polycrystalline SBN (60/40) thin films were coated on silicon and fused silica substrates by a sol-gel process.[28] Preferentially oriented SBN thin films on a fused silica substrate can be formed by applying a dc electric field (about 1 kV/mm) parallel to the surface of the substrate during heat treatment.[29]

In this work SBN thin films on different substrates including silicon, GaAs, and fused silica substrates were made by the sol-gel technique. This process has a number of advantages over conventional techniques such as high homogeneity, ease of composition control, low sintering temperature (about 50% of that of corresponding ceramics), and the possibility of fabricating large-area thin films. Microstructure and physical (pyroelectric, ferroelectric, and optical) properties of these thin films were studied.

II. PROCESSING

SBN thin films studied here were fabricated by the sol-gel method using metal alkoxides as starting materials with purities higher than 95%. The homogeneous solutions were prepared by mixing the metal alkoxides with appropriate compositions. After hydrolysis and polycondensation, when the solution viscosity reaches a desired value, direct dipping or spin-on techniques were used to form thin film of gel on fused silica plates, silicon wafers [n-type (111) wafer with resistivity of 0.0005–0.025 Ω cm and p-type (111) wafer with resistivity of 0.010–0.020 Ω cm], as well as GaAs wafers. The films were then dried and heat treated in air. Heat-treatment temperatures and durations for these ferroelectric thin films were 700–850 °C and 0.5–1 h, respectively. When the final heat treatment was finished, the average film thickness for one single dip in the 0.1-mol/l solution was estimated to be around 1000 Å. A typical flow chart for the fabrication of SBN thin films is shown in Fig. 1. Thicker films may be obtained by repeated cycles of dipping and heat treatment. The thickness of the film was determined by scanning electron microscopy of polished cross sections. Films used in electrical measurements were approximately 0.8 μm in thickness. Differential thermal analysis and x-ray diffraction of sintered thin films suggested that these films were polycrystalline.

For electrical measurements electrodes were made by sputtering Au or evaporating Al onto the corresponding

 ©1991 The American Physical Society

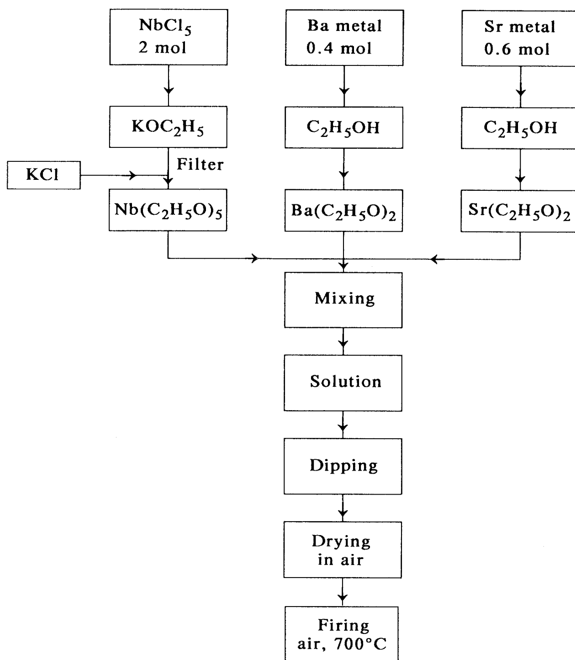

FIG. 1. Typical flow chart for the fabrication of SBN thin films by the sol-gel process.

surface. The other electrode was the silicon (or GaAs) substrate. A metal–ferroelectric film–Si sandwich structure was thus formed. SBN films were also deposited on fused silica substrates to study the microstructure and optical properties. Transparent ferroelectric SBN thin films were obtained on fused silica substrates.

III. MICROSTRUCTURE

Microstructures were studied by x-ray diffraction and direct microscopy. For example, a SBN thin film (with a Sr/Ba ratio of 60/40, heat treated at 750 °C/h, and with a thickness of 0.8 μm) on a silicon substrate had grains with average planar dimensions from 0.3 to 0.8 μm. By using a polarized-light microscope operated in reflecting mode, ferroelectric domain patterns were revealed in the film. Figures 2(a) and 2(b) were taken separately from the same locations in the film on the silicon wafer observed with the light-beam polarization directions perpendicular to each other. Regions of uniform spontaneous polarization within a grain or between several grains, similar to that of PLZT (lead lanthanum zirconate titanate) ceramics,[30] can be observed.

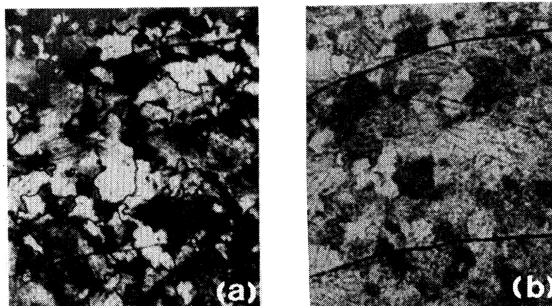

FIG. 2. Micrographs (1000×) of $Sr_{0.60}Ba_{0.40}Nb_2O_6$ thin film (0.8 μm) on a silicon wafer by a polarized-light microscope. The condition of heat treatment of the film is 700 °C by 1 h. (a) and (b) were taken separately with the light-beam polarization directions perpendicular to each other at the same location of the film.

The x-ray-diffraction patterns showed that the lattice structure of the SBN thin films was the same as that of the single crystal (from ASTM x-ray-diffraction data). A preferentially oriented SBN thin film on a fused silica substrate can be formed by applying a dc electric field parallel to the surface of the film during heat treatment. Figure 3 shows the x-ray- (with size 1.5×0.2 cm^2) diffraction patterns of two samples having the same composition and thickness, made by the same process at the same time. One of the samples (lower, without any dc field) shows only random orientation. Another sample (upper) subjected to an applied dc field (about 1 kV/mm) during heat treatment showed enhanced intensities of the lines with low Miller indices on the *c* axis, such as (130), (620), (121), and (131). This result suggests that the lattice planes (130), (620), (121), and (131) lay in the plane of the film surface and the *c* axes in the grains are preferentially oriented in such a way that they are parallel (or nearly parallel) to the direction of the applied dc field. Figure 4 is a representation of the above lattice planes, and it is shown that these planes correspond to the close-packing planes of oxygen atoms in the SBN structure (tungsten-bronze structure).

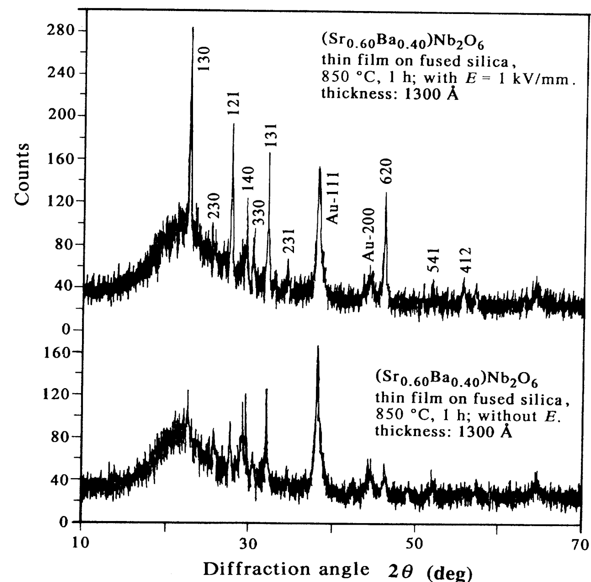

FIG. 3. X-ray-diffraction patterns of SBN thin films with (upper) and without (lower) applying a dc field during heat treatment.

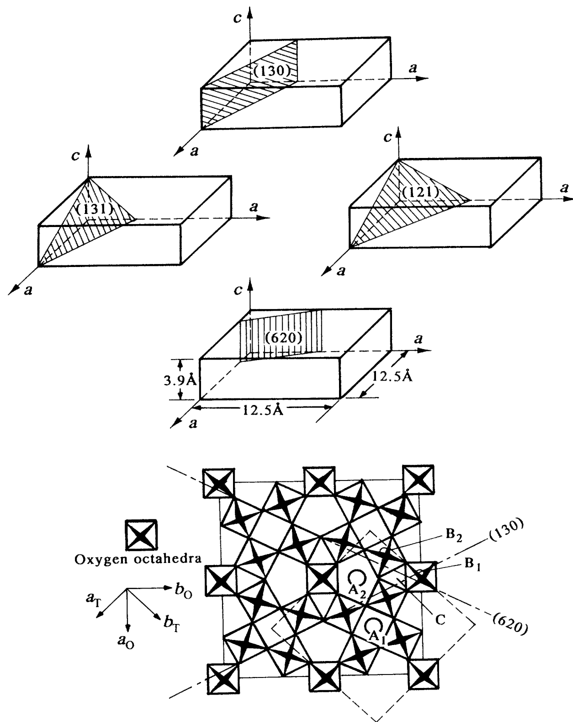

FIG. 4. Schematic illustration of lattice planes (130), (620), (121), and (131) are close-packing planes of oxygen atoms in the SBN structure (tungsten-bronze structure). A basic octahedral framework of the tungsten-bronze structure (looking down the tetragonal and orthorhombic c axis) is shown below.

IV. OPTICAL, DIELECTRIC, PYROELECTRIC, AND FERROELECTRIC PROPERTIES

The optically transparent films were measured in the wavelength range of 0.2–2.5 μm by a Perkin Elmer 330 UV spectrometer. The optical transmission spectrum of SBM films on fused silica substrates is shown in Fig. 5. Refractive indices of 2.31 ± 0.01 were measured on SBN films at a wavelength of 6328 Å by an automatic ellipsometer (Auto El-1I). These data approximate very well with those in single crystals. Therefore, it was concluded

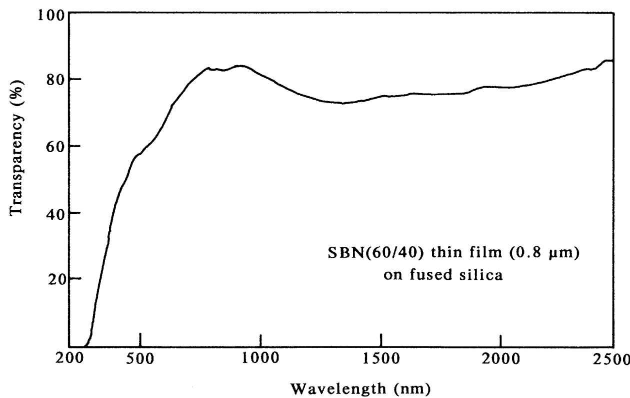

FIG. 5. Optical transition spectrum of SBN thin film (0.8 μm) made by the sol-gel process on a fused silica substrate.

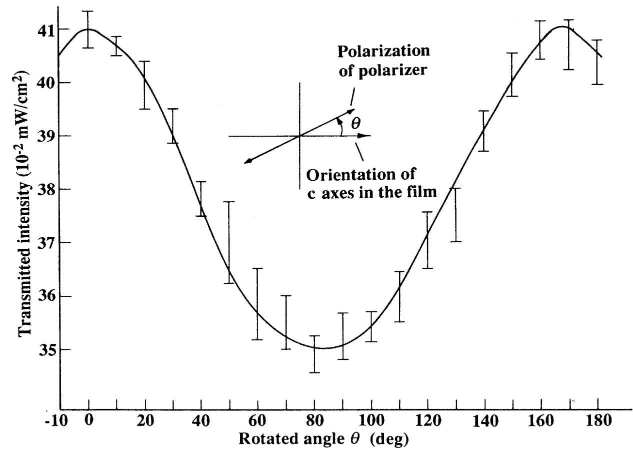

FIG. 6. Optical anisotropy of the preferentially oriented SBN film (0.8 μm) on a fused silica substrate.

that these thin films made by the sol-gel process were highly densified. The optical anisotropy of the preferentially oriented SBN film on a fused silica substrate was observed by putting the SBN film between a detector and a rotatable polarizer which was in front of a light source. The measured result using a light beam with beam diameter of 2 mm is shown in Fig. 6. Note that the minimum in transmitted light intensity is not exactly at 90°. A possible cause is that the average orientation of the **c** axes of the grains covered in the measured area slightly deviates from the average orientation of the **c** axes in the whole film.

Dielectric properties of the SBN thin film were measured on a sample with an Al–SBN thin-film (3000 Å)–GaAs sandwich structure by using a HP-4192A impedance analyzer. The capacitance and the dielectric loss at 1 kHz as a function of temperature are shown in Fig. 7. The change of capacitance in this sample is smaller than that for a single-crystal sample,[19] because the overall observable capacitance is reduced because of the fact that the effective capacitor of the interface heterojunction between the ferroelectric film and semiconductor

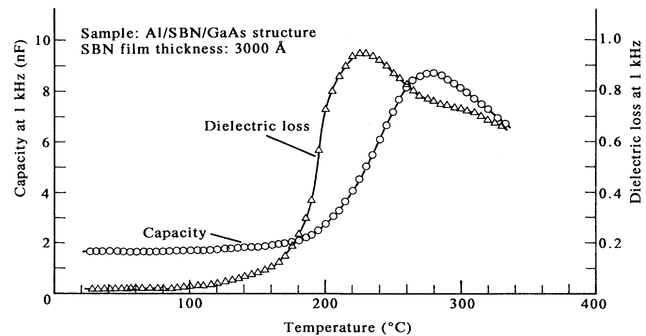

FIG. 7. Dielectric properties of a sample with Al–SBN–GaAs sandwich structure as a function of temperature.

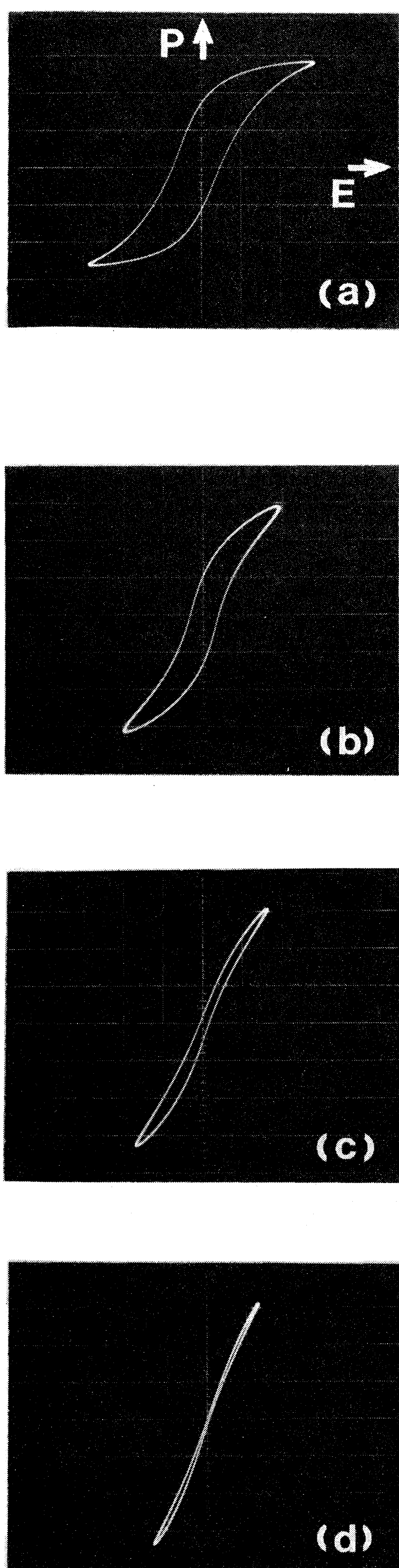

FIG. 8. Ferroelectric **P-E** hysteresis loop of SBN film on GaAs (with doping of Zn, *p*-type conductivity of 640 $\Omega^{-1}\text{cm}^{-1}$). The scale of the x axis (E) is 44 kV/cm/div, and the scale of the y axis (P) is 6.6 μC/cm^2/div. (a) 25 °C, (b) 110 °C, (c) 175 °C, and (d) 200 °C.

substrate is connected in series with the film. From the curves of dielectric properties versus temperature, a diffuse-phase-transition-type ferroelectric-paraelectric phase transition is seen to begin at about 190 °C [see also Fig. 8(d)].

The pyroelectric coefficient was measured with a dynamic method,[19] in which the sample (with Au–ferroelectric film–Si sandwich structure) was heated in the temperature range from 30 to 140 °C, while a pyroelectric current i_p was measured by a picoammeter (417 Keithley Instruments) connected in series with the sample. Before the measurement, the sample of SBN film was poled at 100 °C with a dc electric field of about 2.5 kV/mm. The experimental result was reported in an earlier paper.[31] The pyroelectric coefficient of 2×10^{-8} C/cm^{2}K was obtained at room temperature (27 °C), which is of the same order of magnitude of that of SBN single crystal.[19]

Ferroelectric hysteresis loops of thin films were observed by a modified Sawyer-Tower bridge with an adjustable compensation condenser. Loops and resistivity were measured by a Keithley 196 System DMM multimeter. A symmetric ferroelectric hysteresis loop was observed in the thin films with a pair of parallel Au electrodes sputtered on the surface of the film,[28] and asymmetric loops were observed by using a metal–SBN–GaAs (with low resistivity) sandwich structure (see Fig. 8). As shown in Figs. 8(a)–8(d), the hysteresis loop of the SBN film becomes slimmer when the temperature is increased, and the polarization gradually drops down to zero (in a paraelectric phase) at 200 °C. However, in general, hysteresis loops of ferroelectric thin films on a Si substrate are asymmetric, and the *P-E* loops of film with the same chemical composition on silicon wafers of different conduction type are significantly different.

It is readily seen that in all cases ferroelectric thin films are not ideal insulators but rather semiconductors. We have studied various ferroelectric films on both *n*- and *p*-silicon substrates. *I-V* curves of a metal–ferroelectric film–silicon sandwich structure were observed. These *I-V* curves are similar to that of a *p-n* junction diode. A heterojunction effect has been observed and a theoretical model proposed by the authors has been published.[27]

Photocurrent and photovoltaic effects were demonstrated by using a transparent ITO (indium tin oxide) electrode–ferroelectric film–silicon structure. The measured results of stable photocurrent density and stable photovoltage in a SBN thin film on a silicon substrate are shown in Figs. 9 and 10, respectively. These effects were caused by neither a pyroelectric effect (because pyroelectric current density is in the order of 10^{-8} A/cm^2) nor a photovoltaic effect in a ferroelectric monodomain crystal (since the ferroelectric thin films were not poled, and consequently, the films have a polydomain structure with randomly oriented grains). This result strongly supports the argument that photovoltaic and photocurrent effects were caused by the heterojunction effect at the interface between the ferroelectric thin film and silicon substrate. This newly observed photovoltaic effect of the ferroelectric film–silicon heterojunction offers potential applications in photonic detector devices and solar cell devices.

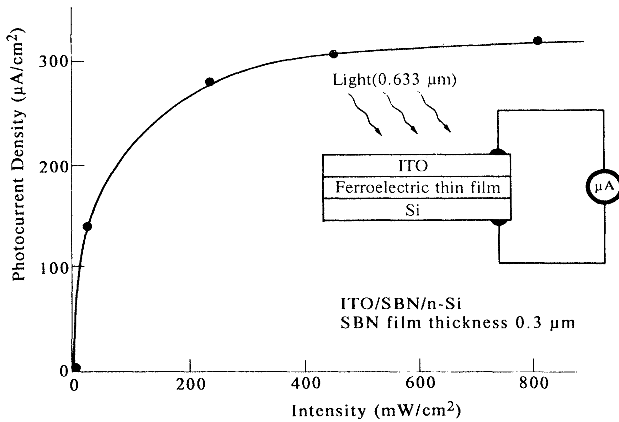

FIG. 9. Stable photocurrent density in SBN thin film on a silicon substrate.

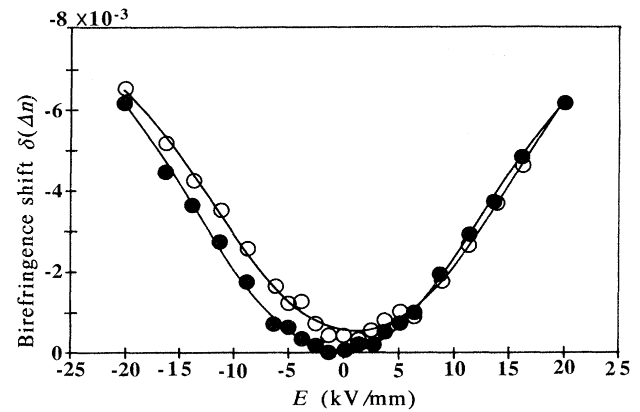

FIG. 11. Measured birefringence shifts in SBN thin film (0.3 μm) as the function of applied electric field **E**. (The curve with solid circles was measured in an unpoled sample and the curve with open circles was measured after the sample was poled.)

V. ELECTRO-OPTICAL PROPERTIES

The electro-optical properties of the SBN (60/40) thin film on fused silica made by the sol-gel process were measured. Planar interdigital electrodes made of 30 nm of chrome and 150 nm of gold were deposited on the film surfaces using *e*-beam evaporation and photolithographic lift-off techniques. The electrode width and gap are both 8 μm. A dc voltage was applied across the electrodes. The birefringence shifts in the films, $\Delta n = n(\mathbf{P}\|\mathbf{E}) - n(\mathbf{P}\perp\mathbf{E})$, where **P** is the polarization of light, were measured using a phase-modulation detection method in conjunction with a transmission cofocal scanning polarization microscope.[14] The polarization state of the incoming light was phase modulated by a photoelastic modulator. The final output signal detected by the lock-in amplifier is $I = A\sin^2(\Delta\theta)$, where A is a calibration constant and $\Delta\theta$ is the phase retardation. The smallest retardation which could be measured was 3×10^{-5} deg. The condensing lens of the microscope can focus the incident light down to a 0.4-μm-diameter spot in the film, and the electro-optic (EO) effects of the small spot were studied. The light source used was filtered mercury light at 577 nm.

The birefringence (Δn) was calculated from

$$\Delta n = \lambda\Delta\theta/\pi d \ , \tag{1}$$

where λ is the wavelength of the incident light and d is the film's thickness. The measured birefringence shifts in an unpoled SBN film with the thickness of 0.3 μm as a function of the applied electric field E and a function of E^2 are shown in Figs. 11 and 12, respectively. The electric field can induce ferroelectric domain realignment, anisotropy change, nonlinear dielectric or ionic polarization change, or phase transition, and thus effects of various orders may appear. As shown, the curves present neither linear nor quadratic behavior and the remanent birefringence is caused by poling action after the large dc field was applied to the film.

The birefringence shifts can be represented by using the following polynomial expansion of the applied elec-

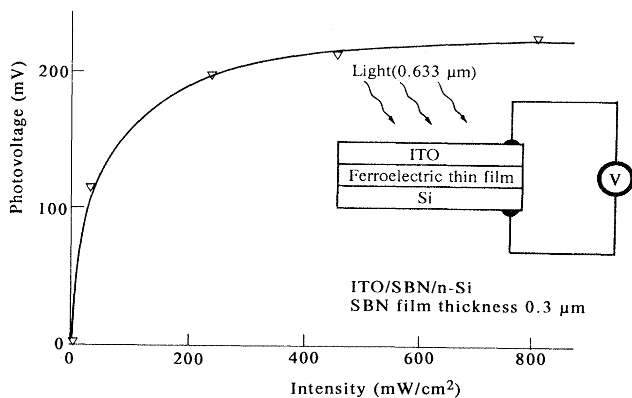

FIG. 10. Stable photovoltage in SBN thin film on a silicon substrate.

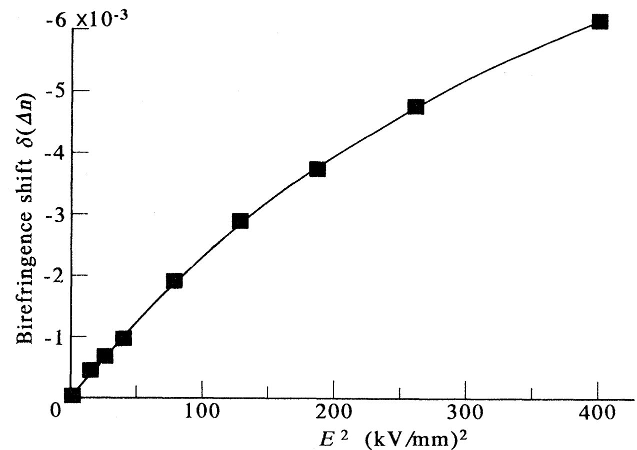

FIG. 12. Measured birefringence shifts in SBN thin film (0.3 μm) as the function of the square of the applied electric field $\mathbf{E}^2$.

TABLE I. Polynomial fits of electro-optic effect in SBN thin film made by the sol-gel method.

Experimental curve in Fig. 11	a_0 (10^{-4})	a_1 (10^{-11} m/V)	a_2 (10^{-17} m^2/V^2)	a_3 (10^{-25} m^3/V^3)	a_4 (10^{-32} m^4/V^4)
(from −20 to +20 kV/mm)	−0.795	−1.65	−2.28	0.385	1.93
(from +20 to −20 kV/mm)	−5.25	4.92	−2.14	−1.05	1.77

tric field E up to four terms:

$$\delta(\Delta n)=a_0+a_1E+a_2E^2+a_3E^3+a_4E^4 , \quad (2)$$

where a_0 is the remanent birefringence. The remanent birefringence corresponds to the remanent polarization of ferroelectrics after the sample was poled by an applied dc field with the field removed. The coefficients a_0, a_1, a_2, a_3, and a_4 in Eq. (2) for the experimental curve of the unpoled sample (when the applied field changed from −20 to +20 kV/mm for the first half of the cycle, represented by solid circles) and for the experimental curve of the poled sample (when the applied field changed from +20 to −20 kV/mm to complete the measurement cycle, represented by open circles) are listed in Table I. Apparently, remanent birefringence a_0 and the coefficients in terms of odd powers of E (a_1 and a_3) in the poled sample are much larger than those in the unpoled sample. That is because a_0, a_1, and a_3 of ferroelectric materials are related to the dielectric and optical anisotropies, which could be enhanced by an applied field on the sample. However, a_2 and a_4, the coefficients in terms of even powers of E, are almost the same in both curves owing to the fact that these coefficients are independent of the anisotropy of the electro-optic material.

Usually, for the convenience of application, the transverse effective linear electro-optic coefficient r_c (after poling and when E is enough small) can be calculated approximately from the change in birefringence using the equation

$$r_c=2\delta(\Delta n)/n^3E \quad \text{(when } E \text{ is small)} , \quad (3)$$

where n is the refractive index of the film. The effective linear electro-optic coefficient r_c of the poled sample calculated, as shown by the open circles in Fig. 11, from Eq. (3) was approximately 30×10^{-12} m/V using 2.3 as the value of the refractive index and the birefringence change obtained from the curve in Fig. 11 at small dc field (<2 kV/mm). Even though the refractive index of the SBN film is almost the same as single crystals, the dielectric and optical anisotropies (corresponding to the coefficient a_1 and the optical birefringence) of a polycrystalline film should be smaller than those of a single crystal. It is therefore expected that r_c, which depends on the dielectric and optical anisotropies of the ferroelectric materials, to be smaller than those of the SBN single crystal.[20]

VI. SUMMARY

(1) Transparent, crack-free polycrystalline, and ferroelectric SBN thin films on a fused silica substrate have been fabricated by the sol-gel process.

(2) Preferentially oriented SBN thin films on a fused silica substrate can be formed by applying a dc electric field (about 1 kV/mm) parallel to the surface of the substrate during heat treatment.

(3) A heterojunction effect in the sandwich structure of metal–ferroelectric film–silicon discovered from the measurement of I-V curves has been further confirmed by the demonstration of photovoltaic and photocurrent effects.

(4) The optical refractive index (=2.31) of the SBN thin film by the sol-gel process is close to that in single crystal. The pyroelectric coefficient and linear electric-optic coefficient of the SBN thin film are smaller than those in single crystal. However, these coefficients are of the same order of magnitude as those in single crystal and certainly larger than some of the other ferroelectric crystals, such as $LiNbO_3$ and $LiTaO_3$.

ACKNOWLEDGMENTS

This work was supported by the Air Force Office of Scientific Research, Directorate of Chemical and Atmosphere Sciences under Grant No. AFOSR-88-0066. The authors also wish to thank Ken C. Cheng and N. Desimone for their help in part of the experiments in this work. We also thank Dr. Adam Y. Wu and Feiling Wang, Department of Physics, University of New Mexico for the measurement of the electro-optic effect in SBN thin films.

[1]M. Minakata *et al.*, J. Appl. Phys. **50**, 7898 (1979).
[2]N. F. Foster, J. Appl. Phys. **40**, 420 (1969).
[3]R. N. Castellans and L. G. Feinstein, J. Appl. Phys. **50**, 4406 (1979).
[4]A. M. Glass, Phys. Rev. **172**, 564 (1968).
[5]H. P. Beerman, Ferroelectrics **2**, 123 (1971).
[6]A. M. Glass and R. L. Abrams, J. Appl. Phys. **41**, 4455 (1970).
[7]D. W. Chapman, J. Vac. Sci. Technol. **9**, 425 (1972).
[8]R. B. Atkin, Ferroelectrics **3**, 213 (1971).
[9]S. Y. Wu, W. J. Takei, M. N. Francombe, and S. E. Cummins, Ferroelectrics **3**, 217 (1972).
[10]D. W. Chapman, in *Proceedings of the IEEE International Computer Group Conference, 1970, Washington, D.C.*, edited by H. D. Huskey and J. Kinkley (IEEE, New York, 1970), p. 56.
[11]D. W. Chapman and P. R. Mehta, Ferroelectrics **3**, 101 (1972).
[12]P. R. Mehta, Ferroelectrics **4**, 5 (1972).
[13]J. C. Webster and F. Zernike, Ferroelectrics **10**, 249 (1976).

[14]A. Y. Wu, Feiling Wang, Ching-Bo Juang, and Carlos Bustamante, in *Ferroelectric Thin Films,* edited by E. R. Myers and A. I. Kingon, MRS Symposia Proceedings No. 200 (Materials Research Society, Pittsburgh, 1990), p. 261.
[15]S. Y. Wu, Ferroelectrics **11**, 379 (1976).
[16]Shu-Yau Wu, IEEE Trans. Electron Devices **ED-21**, 499 (1974).
[17]S. K. Dey and R. Zuleeg, Ferroelectrics **108**, 37 (1990).
[18]L. Eric Cross, in *Proceedings, IEEE Micro Electromechanical Systems, Napa Valley, CA, 1990,* edited by J. E. Wood and R. T. Howe (IEEE, New York, 1990), p. 72.
[19]A. M. Glass, J. Appl. Phys. **40**, 4699 (1969); **41**, 2268(E) (1970).
[20]S. Sakamoto and T. Yazaki, Appl. Phys. Lett. **22**, 429 (1973).
[21]F. Micheron and G. Bismuth, Appl. Phys. Lett. **23**, 71 (1973).
[22]J. D. Zook and S. T. Liu, J. Appl. Phys. **49**, 4604 (1978).
[23]Liu Wen-Hu *et al.*, Opt. Commun. **64**, 81 (1987).
[24]Haiying Xu, Kebin Xu, Yuhuan Xu, Huanchu Chen *et al.*, Proc. SPIE **1220**, 64 (1990).
[25]E. J. Sharp, M. J. Miller, G. L. Wood, W. W. Clark III, G. J. Salamo, and R. R. Neurgaonkar, in *Proceedings of the Sixth IEEE International Symposium on Applications of Ferroelectrics (ISAF'86),* Bethelem, 1986, edited by V. E. Wood (IEEE Publishing Services, New York, 1986), pp. 51–56.
[26]V. G. Zhdanov *et al.*, Ferroelectrics **29**, 219 (1980).
[27]Yuhuan Xu, Ching-Jin Chen, Ren Xu, and J. D. Mackenzie, J. Appl. Phys. **67**, 2985 (1990).
[28]Ren Xu, Yuhuan Xu, Ching-Jin Chen, and J. D. Mackenzie, J. Mater. Res. **5**, 916 (1990).
[29]Yuhuan Xu, Ching-Jin Chen, Ren Xu, and J. D. Mackenzie, in *Ferroelectric Thin Films* (Ref. 14), p. 13.
[30]G. H. Haertling, Ferroelectrics **75**, 25 (1987).
[31]Ching-Jih Chen, Yuhuan Xu, Ren Xu, and J. D. Mackenzie, J. Appl. Phys. **69**, 1763 (1991).

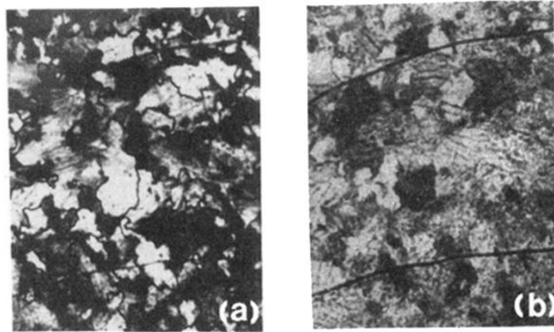

FIG. 2. Micrographs (1000×) of $Sr_{0.60}Ba_{0.40}Nb_2O_6$ thin film (0.8 μm) on a silicon wafer by a polarized-light microscope. The condition of heat treatment of the film is 700 °C by 1 h. (a) and (b) were taken separately with the light-beam polarization directions perpendicular to each other at the same location of the film.

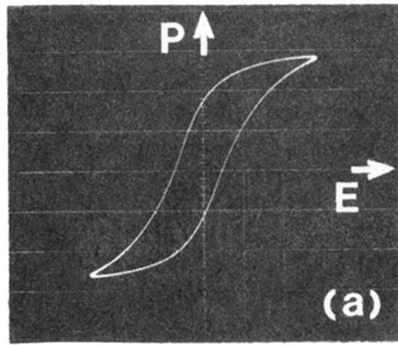

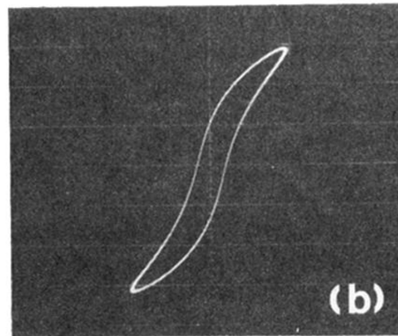

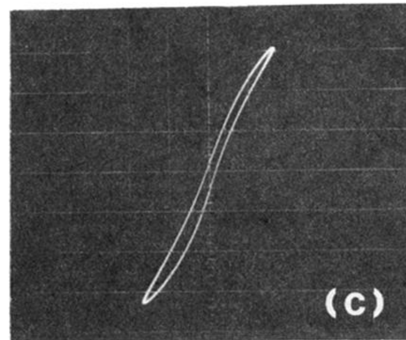

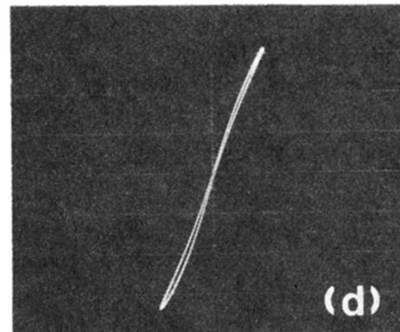

FIG. 8. Ferroelectric **P-E** hysteresis loop of SBN film on GaAs (with doping of Zn, p-type conductivity of 640 $\Omega^{-1}\,cm^{-1}$). The scale of the x axis (E) is 44 kV/cm/div, and the scale of the y axis (P) is 6.6 $\mu C/cm^2$/div. (a) 25 °C, (b) 110 °C, (c) 175 °C, and (d) 200 °C.